

Discovery of twin kHz quasi-periodic oscillations in the low-mass X-ray binary XTE J1701–407

Devraj D. Pawar,^{1*} Maithili Kalamkar,² Diego Altamirano,² Manuel Linares,³
K. Shanthi,⁴ Tod Strohmayer,⁵ Dipankar Bhattacharya⁶ and Michiel van der Klis²

¹Ramniranjan Jhunjhunwala College, Ghatkopar, Mumbai 400086, India

²Astronomical Institute ‘Anton Pannekoek’, University of Amsterdam, Science Park 904, NL-1098XH Amsterdam, the Netherlands

³Instituto de Astrofísica de Canarias, c/Vía Láctea s/n, E-38205 La Laguna, Tenerife, Spain

⁴UGC Academic Staff College, University of Mumbai, Mumbai 400098, India

⁵Astroparticle Physics Laboratory, Mail Code 661, NASA Goddard Space Flight Center, Greenbelt, MD 20771, USA

⁶Inter University Centre for Astronomy and Astrophysics, Pune 411007, India

Accepted 2013 May 21. Received 2013 May 17; in original form 2013 April 9

ABSTRACT

We report the discovery of kHz quasi-periodic oscillations (QPOs) in three *Rossi X-ray Timing Explorer* observations of the low-mass X-ray binary XTE J1701–407. In one of the observations we detect a kHz QPO with a characteristic frequency of 1153 ± 5 Hz, while in the other two observations we detect twin QPOs at characteristic frequencies of 740 ± 5 , 1112 ± 17 Hz and 740 ± 11 , 1098 ± 5 Hz. All detections happen when XTE J1701–407 was in its high-intensity soft state, and their single-trial significance is in the 3.1 – 7.5σ range. The frequency difference in the centroid frequencies of the twin kHz QPOs (385 ± 13 Hz) is one of the largest seen till date. The 3–30 keV fractional rms amplitude of the upper kHz QPO varies between ~ 18 and ~ 30 per cent. XTE J1701–407, with a persistent luminosity close to 1 per cent of the Eddington limit, is among the small group of low-luminosity kHz QPO sources and has the highest rms for the upper kHz QPO detected in any source. The X-ray spectral and variability characteristics of this source indicate its atoll source nature.

Key words: binaries: general – stars: individual: XTE J1701–407 – stars: neutron – X-rays: binaries.

1 INTRODUCTION

Low-mass X-ray binaries (LMXBs) can be divided into systems containing a black hole candidate and those containing a neutron star (NS). The accretion properties of these systems can be studied through the timing and spectral properties of the X-ray emission (e.g. van der Klis 1995a; Ford et al. 2000; Wijnands & Miller 2002). On the basis of correlated variations in the X-ray colour–colour diagram (CD) and power density spectra (PDS), the NS LMXBs are classified as *Z* sources and *atoll* sources (Hasinger & van der Klis 1989). The *Z* sources are generally high-luminosity sources (0.5 – 1.0 of Eddington luminosity L_{Edd}) while the *atoll* sources are low-luminosity sources (0.01 – $0.5L_{\text{Edd}}$; see, e.g., van der Klis 2006b for a review, and Homan et al. 2010 for recent discoveries).

In the CD the *atoll* sources show three distinct states: the extreme island state (EIS), the island state (IS) and the banana state, the latter is further subdivided into the lower-left banana (LLB), lower banana (LB) and the upper banana (UB). In Fig. 1, we show the CD of the well-known *atoll* source 4U 1608–52 (e.g. van Straaten,

van der Klis & Méndez 2003), where all the different *atoll* spectral states are seen. Generally, as the source moves from the EIS to the UB through the IS, LLB and LB, the spectrum softens and the soft X-ray intensity increases (see, e.g., Di Salvo, Méndez & van der Klis 2003; Schnerr et al. 2003).

A number of quasi-periodic oscillations (QPOs) and broad-band variability components are often present simultaneously in the PDS of the X-ray light curves of these systems. The timing characteristics of these variability components are related to the spectral state of the source, i.e. to the position of the source in the CD. Generally, the characteristics of the timing features [i.e. frequency, quality factor and fractional root-mean-square (rms) amplitude] vary monotonically as the source moves along the *atoll* track. This behaviour has been attributed to changes in the accretion rate (\dot{M}), the interaction of the matter in the accretion disc and the radiation emitted from the region close to the NS surface which affects the X-ray variability and spectrum (e.g. van der Klis 2006a for a review). QPOs can be seen with frequency between a few mHz to more than a kHz. Broad-band components are only seen up to ~ 100 – 200 Hz. Weak band-limited noise is seen in the power spectra of *atoll* sources when they are in the banana state. This noise becomes stronger as the source spectrum hardens, i.e. as the source moves to the ISS.

* E-mail: devrajdp@gmail.com

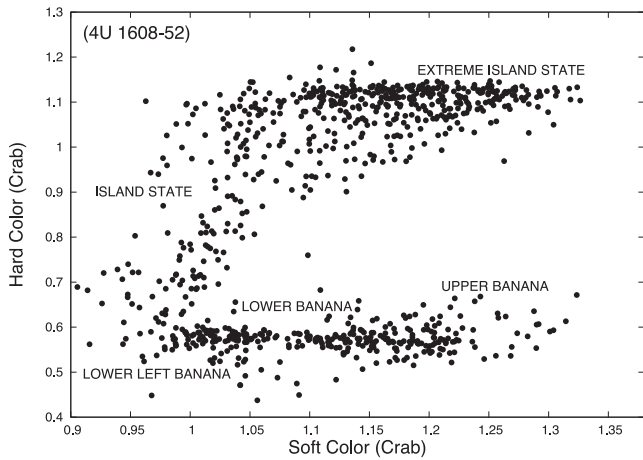


Figure 1. CD of the atoll source 4U 1608–52 plotted using observations obtained over 14 years. Each point represents the averaged colour per observation (bands are defined as in Section 2.1). The error bars are of the order of the size of the symbols. In this CD all the spectral states are observed. The kHz QPOs are usually observed in the LB states.

Usually, one or two kHz QPOs are detected in the LLB and the LB. No kHz QPOs are generally detected in the UB nor in the harder EIS states (van der Klis 2000, 2006b; Altamirano et al. 2008b). In the hard ISs, two broad features have been suggested as the equivalent of kHz QPOs at low frequencies ($\lesssim 400$ Hz; e.g., Psaltis, Belloni & van der Klis 1999; van Straaten, van der Klis & Wijnands 2004, 2005, and references therein).

The Keplerian velocities in the intense gravitational fields near NSs are very high. Accreting matter therefore has very short (millisecond) orbital periods which may be the cause of the kHz QPOs. In some models (e.g. Miller, Lamb & Psaltis 1998; van der Klis 2000; Lamb & Miller 2003; Lee, Abramowicz & Kluźniak 2004) and observations (e.g. Jonker, Méndez & van der Klis 2002; Markwardt & Swank 2003; Wijnands et al. 2003; Linares et al. 2005), the difference in the frequency of the twin kHz QPOs ($\Delta\nu$) is thought to be related to the NS spin frequency (ν_s) as $\Delta\nu \simeq \nu_s$ or $\Delta\nu \simeq \nu_s/2$. However, current data do not allow a definitive statement about this (see, e.g., Méndez & Belloni 2007; Yin et al. 2007; van der Klis 2008; Altamirano et al. 2010).

The *Rossi X-ray Timing Explorer* (*RXTE*) has been one of the most successful X-ray astronomy missions. From 1995 to 2012, *RXTE* has been used for observing known X-ray sources and also for discovering many new ones. An example of the latter is XTE J1701–407, a transient X-ray source discovered with *RXTE* on 2008 June 8 (Markwardt, Pereira & Swank 2008). Since its discovery XTE J1701–407 has shown thermonuclear X-ray bursts (Falanga et al. 2009; Linares et al. 2009; Chenevez et al. 2010) establishing that it is an accreting NS. The discovery of kHz QPOs was briefly reported by Strohmayer, Markwardt & Swank (2008), where it was suggested that this source is among the least luminous sources ($L_X = 0.01L_{\text{Edd}}$) in which twin kHz QPOs have been detected. Triggered by this possibility, in this paper we present a detailed study of the X-ray spectral and variability characteristics of XTE J1701–407 using all the 58 *RXTE* observations.

The upper limit on the distance of XTE J1701–407 was set as 6.1 kpc by Linares et al. (2009) and Falanga et al. (2009) from the spectral evolution of a long type I X-ray burst. Later, Chenevez et al. (2010) reported detection of photospheric expansion during a burst and derived the distance to XTE J1701–407 to be 5.0 ± 0.4 kpc; we use this distance for estimating L_X .

2 OBSERVATIONS AND DATA ANALYSIS

2.1 Light curves and CD

To study the long-term ($>$ days) X-ray variability, we use *RXTE* Proportional Counter Array (PCA; see Zhang et al. 1993; Jahoda et al. 2006) Galactic bulge scan monitoring observations (Swank & Markwardt 2001); the observations were taken once every ~ 3 d; the intensity (in units of cts/sec/5PCUs) is provided in the 2–10 keV energy range.

To study the X-ray spectral variations and the short-term variability ($<$ seconds), we use the 58 pointed observations obtained with the *RXTE* PCA between 2008 June 9 and 2011 September 20. Each observation is between 0.5 and 17 ks long, adding up to a total of ~ 235.7 ks. For details on the observations, see Table 1. We calculated X-ray colours using 16 s time resolution Standard 2 mode data. Light curves were cleaned for instrumental effects like spikes and dropouts, and corrected for background contribution in each band using the standard faint source background model for the PCA (for details of the model, see PCA Digest at <http://heasarc.gsfc.nasa.gov/>).

We define the soft colour as the ratio of average count rates per observation in the energy ranges 3.6–6.4 and 2.0–3.5 keV, the hard colour as the ratio of count rates in the energy ranges 9.7–16.0 and 6.4–9.7 keV, and the intensity as the count rate in the energy range 2–16 keV. The exact count rates in these energy bands were obtained by linearly interpolating between PCU channels. To correct for the difference in sensitivity between different PCUs, we normalized the count rates in each energy band by those of the Crab nebula in the same energy bands (e.g. Kuulkers et al. 1994; van Straaten et al. 2003). The Crab nebula observations used are those closest in time to each XTE J1701–407 observation. Given that the spectra of the source did not vary significantly within an observation (even in the long 17 ks observation), in this paper we report intensities and colours per observation.

2.2 Fourier timing analysis

We used 122 μ s time resolution Event mode data available for 39 observations between 2008 June 9 and September 29. For the remaining 19 observations (2010 to 2011), the data are available in the Good Xenon mode which has a resolution of ~ 1 μ s. These data were binned to also obtain a resolution of ~ 122 μ s which results in a Nyquist frequency of 4096 Hz.

From the event list of each observation, we calculate the power spectra using fast Fourier transforms (FFTs) of continuous 16 s data segments (leading to a minimum frequency of $1/16$ s = 0.0625 Hz) and using data in the 3–30 keV energy range (so as to optimize the signal-to-noise ratio). The 16 s power spectra are then averaged to get one power density spectrum per observation. In order to search for QPOs at very low frequencies, we also calculate FFTs of 1024 s data segments, which gives a minimum frequency of $1/1024$ s = 0.976 mHz. In both cases, no dead time or background corrections are done before calculating the power density spectrum. We estimate the dead time corrected Poisson noise spectrum using the analytic function in Zhang et al. (1995). The estimated Poisson noise spectrum is subtracted from the power density spectrum which is then converted to rms normalization (van der Klis 1995b). In the rms normalization, the square root of the integrated power gives the fractional rms amplitude of the source variability in the frequency range over which we integrate.

Table 1. Observations of XTE J1701–407.

Observation	Date (mm/dd/yy)	Exposure (s)	Counts ^a (c/s/PCU)	State ^b
93444-01-01-00	06/09/08	1027	17.8	H
93444-01-01-01	06/10/08	2655	20.5	H
93444-01-02-00	06/16/08	2039	39.6	S
93444-01-02-01	06/17/08	2659	27.1	H
93444-01-02-02	06/18/08	1964	25.8	H
93444-01-03-00	06/23/08	3493	17.4	H
93444-01-03-01	06/21/08	3561	20.3	H
93444-01-03-02	06/22/08	3102	20.0	H
93444-01-04-00	07/18/08	3510	41.7	S
93444-01-04-01	07/22/08	1984	42.9	S
93444-01-04-02	07/23/08	3541	45.2	S
93444-01-05-00	07/25/08	2004	39.4	S
93444-01-05-01	07/27/08	1820	40.1	S
93444-01-05-02	07/30/08	3838	37.8	S
93444-01-05-03	07/31/08	3602	32.3	S
93444-01-06-00	08/02/08	2126	31.2	S
93444-01-06-01	08/05/08	3784	12.1	H
93444-01-06-02	08/01/08	3536	32.8	S
93444-01-06-03	08/03/08	4166	25.5	S
93444-01-06-04	08/04/08	7767	13.9	H
93444-01-06-05	08/06/08	1888	10.2	H
93444-01-06-06	08/07/08	1562	9.4	H
93444-01-07-00	08/08/08	2647	8.1	H
93444-01-07-01	08/09/08	2761	8.9	H
93444-01-07-02	08/10/08	2402	11.9	H
93444-01-07-03	08/12/08	2300	13.1	H
93444-01-07-04	08/13/08	1821	15.3	H
93444-01-07-05	08/14/08	5361	15.5	H
93444-01-07-06	08/09/08	635	8.7	H
93444-01-07-07	08/09/08	2216	10.5	H
93444-01-07-08	08/14/08	1760	13.4	H
93444-01-07-09	08/14/08	1342	15.1	H
93444-01-08-00	08/18/08	493	17.9	H
93444-01-09-00	09/12/08	1657	57.2	S
93444-01-09-01	09/14/08	1943	81.7	S
93444-01-09-02	09/15/08	555	22.5	H
93444-01-09-03	09/16/08	2147	25.6	H
93444-01-09-04	09/18/08	2107	21.8	H
93444-01-10-00	09/20/08	2765	22.3	H
95328-01-01-00 ^b	01/05/10	13 695	33.4 ^b	–
95328-01-01-01 ^b	01/05/10	3457	35.7 ^b	–
95328-01-01-02 ^b	01/07/10	1278	32.0 ^b	–
95328-01-01-03 ^b	01/07/10	1293	32.3 ^b	–
95328-01-01-04 ^b	01/07/10	5738	44.3 ^b	–
95328-01-02-00 ^b	01/08/10	10 422	45.1 ^b	–
95328-01-03-00 ^b	03/29/10	6969	61.9 ^b	–
95328-01-04-00 ^b	05/24/10	11 446	25.6 ^b	–
95328-01-05-00 ^b	08/16/10	3562	56.7 ^b	–
95328-01-06-00 ^b	08/17/10	3578	54.5 ^b	–
95328-01-07-00 ^b	11/14/10	10 302	22.4 ^b	–
95328-01-08-00 ^b	01/06/11	3390	70.7 ^b	–
95328-01-08-01 ^b	01/05/11	1439	85.1 ^b	–
95328-01-09-00 ^b	01/18/11	10 326	23.2 ^b	–
95328-01-09-01 ^b	01/18/11	17 179	27.6 ^b	–
95328-01-10-00 ^b	04/25/11	7190	16.6 ^b	–
95328-01-10-01 ^b	04/26/11	7305	16.7 ^b	–
95328-01-10-02 ^b	04/28/11	9590	18.0 ^b	–
95328-01-11-00 ^b	09/20/11	7073	20.6 ^b	–

^aThe count rate is in the 3–30 keV range and averaged per PCU after subtracting the background counts.^bH and S indicate hard- and soft-state observations, respectively; the observations indicated by ‘–’ are not used for colour analysis due to contamination by the OAO 1657–415 flux (Section 2.3).

We fit the power density spectrum using multiple Lorentzian components. The characteristic frequency of the Lorentzians is given by $\nu_{\max} = \sqrt{\nu_0^2 + (\text{FWHM}/2)^2} = \nu_0 \sqrt{1 + 1/(4Q^2)}$ (Belloni, Psaltis & van der Klis 2002). The quality factor is defined as $Q = \nu_0/\text{FWHM}$. FWHM is the full width at half-maximum and ν_0 is the centroid frequency of the Lorentzian. The Lorentzian components are usually categorized according to their characteristic frequencies as upper kHz (L_u), lower kHz (L_ℓ), hump (L_h), break (L_b) and hectohertz (L_{hHz}) (e.g., Belloni et al. 2002; van Straaten et al. 2003; Altamirano et al. 2005). The quoted errors use $\Delta\chi^2 = 1.0$. Where only one error is quoted, it is the quadratic average between the positive and the negative error.

2.3 Contaminated observations

Of the 58 *RXTE* observations, the first 39 observations, performed in 2008 (proposal P93444), were obtained with an RA–Dec. pointing of 255°35′, –40°5′ and the later 19 observations, performed in 2010–2011 (proposal P95328), were obtained with an RA–Dec. pointing of 255°43′, –40°86′. During the 2008 observations, the high-mass X-ray binary (HMXB) pulsar OAO 1657–415 was at $\sim 1^\circ 17'$ from the PCA pointing coordinates, whereas during the 2010–2011 ones the HMXB was at $\sim 0^\circ 83'$. Therefore, in the latter case, the HMXB is in the 1° FWHM field of view (FoV) of the *RXTE*-PCA observations of XTE J1701–407. To explore whether OAO 1657–415 affected our observations, we created 1024 s length power spectra of all 2010–2011 observations. In observations 95328-01-01-04, 95328-01-02-00, 95328-01-03-00 and 95328-01-04-00, we find a very narrow peak which has a frequency of 27.2 mHz. A period search using the `FTOOL` *efsearch* reveals a strong signal at 37.063 s corresponding to a frequency 26.981 mHz. This is consistent with the spin period of OAO 1657–415 (Barnstedt et al. 2008; Denis, Bulik & Marcinkowski 2010). Given that the 2010–2011 observations are clearly contaminated by the flux from OAO 1657–415, we do not use them in the CD or intensity plots but we do use them in our timing analysis, as no high-frequency features ($\gtrsim 1.27$ Hz) have ever been detected from HMXBs (Kaur et al. 2007, and references therein). We also analysed all the 86 *RXTE* observations of OAO 1657–415 for the presence of kHz QPOs and detected none.

3 RESULTS

3.1 Light curve and CD

In the upper panel of Fig. 2, we show the bulge scan long-term light curve of XTE J1701–407. After the outburst onset (detected on 2008 June 8, MJD 546 25), the light curve shows instances of increased emission on top of an average 2–10 keV intensity of ~ 100 cts/s/5PCU, during which the intensity increases to nearly two to four times the average. After a 3 yr long outburst since its discovery, the source went below the *RXTE* Galactic bulge scan monitor detection limit around 2011 August 27 (Degenaar et al. 2011a). A few days later, it rebrightened to ~ 100 cts/s/5PCU from 2011 September 16 to 24 (Degenaar et al. 2011b); after that its intensity decreased to ~ 10 cts/s/5PCU and remained so till it was last monitored by *RXTE* on 2011 October 29 (MJD 558 63.4). In the lower panel of Fig. 2, we show the Crab normalized light curve for 2008 observations. These observations sample the source when its intensity was between ~ 2 and ~ 25 mCrab. In Fig. 3, we show the CD of the 2008 observations. It is clear that the observations are confined to a few distinct regions in the diagram. We refer to the 27

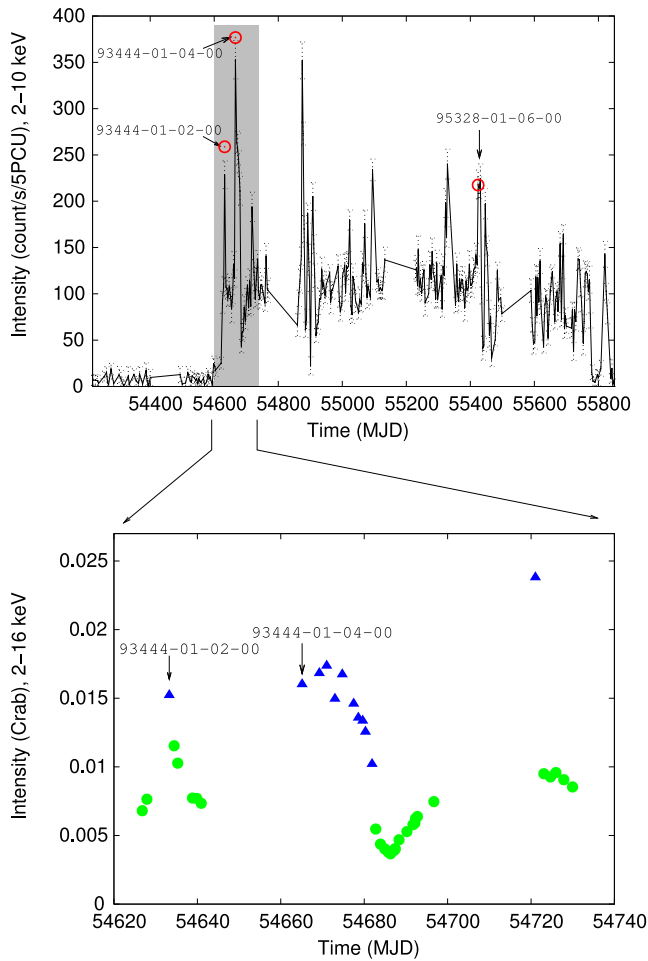


Figure 2. Top panel: long-term light curve of XTE J1701–407 obtained from the PCA Galactic bulge scan monitoring observations. The arrows and circles mark the approximate times and intensities of the observations in which kHz QPOs are detected. The circles are offset from the PCA scan points as they represent the average count rate per pointed observation. The grey shadow marks the period in 2008 when 39 *RXTE* pointed observations were performed. The period when the 19 *RXTE* pointed observations obtained from 2010 January 5 to 2011 September 20 were performed is indicated by the dashed line in the upper-right part of the panel. Bottom panel: normalized light curve of the 39 pointed observations performed in 2008. The error bars are of the order of the size of the symbols. The green circles and blue triangles mark when the source was in the hard and soft state, respectively (see also Fig. 3). We do not show the remaining 19 observations as their intensity/colours are contaminated by the flux of an HMXB, see Section 2.3.

observations with hard colour $\gtrsim 0.75$ as hard state (circles) and the 12 observations with hard colour $\lesssim 0.75$ as soft state (triangles).

As can be seen in Fig. 2, the first two pointed observations of XTE J1701–407 occur when it was in the hard state (on MJD 546 26 and 546 27). Then the source was detected in the high-luminosity soft state on MJD 546 33 in one observation. As the intensity decreased, the source went to the hard state again where it was observed for ~ 5 d. After a gap of ~ 27 d, XTE J1701–407 was observed in the soft state for ~ 17 d after which its L_X decreased and underwent a transition to the hard state; our data cover ~ 14 d before they stop. After an ~ 25 d gap, the source was in the soft state for 1 d (MJD 547 21); within a day XTE J1701–407 transitioned to the hard state again. Clearly, the soft-state observations track the high-intensity periods; however, there is no clear intensity cut that

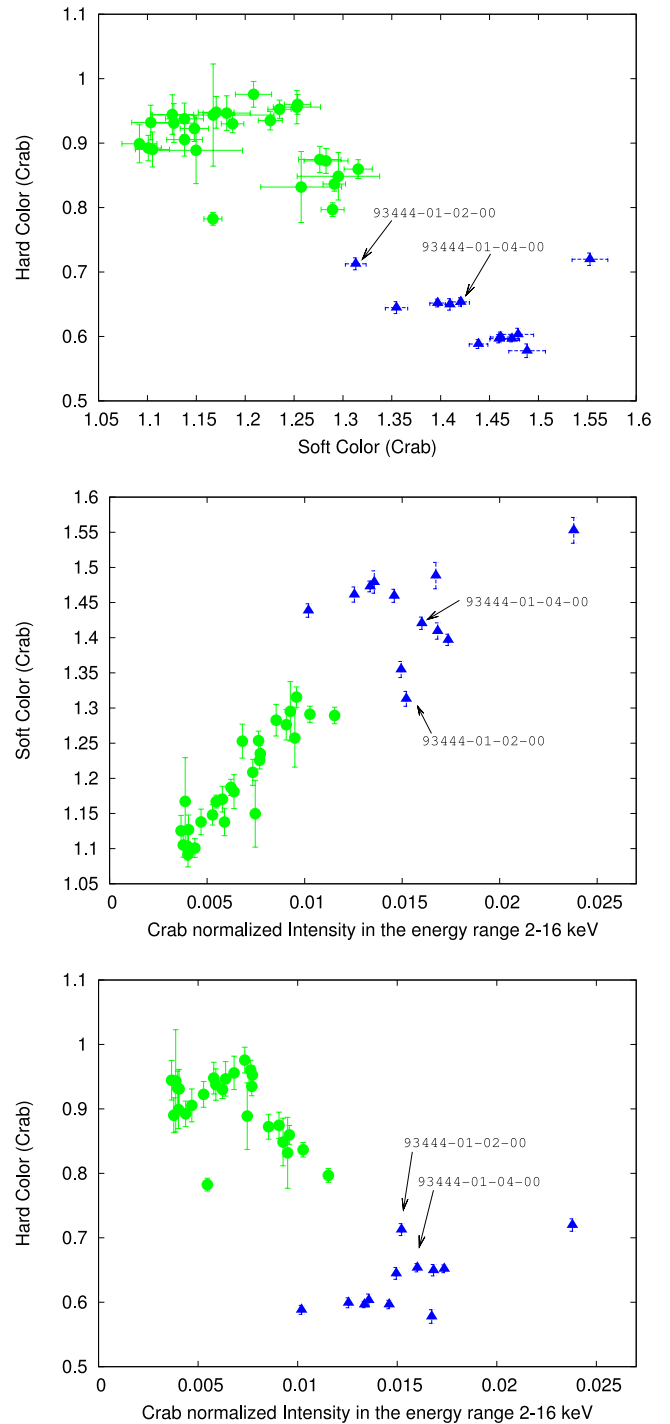


Figure 3. Top panel: CD of XTE J1701–407 using the 39 pointed *RXTE* observations performed in 2008. The arrows indicate observations in which the kHz QPOs are detected. The green circles and blue triangles mark the hard-state (low L_X) and the soft-state (high L_X) observations, respectively. Comparing with Fig. 1, the hard-state observations lie in the lower region of the *IS* while the soft-state observations correspond to the *banana state*. Middle panel: soft colour versus intensity diagram. Bottom panel: hard colour versus intensity diagram. The spectrum becomes softer as the L_X increases. The kHz QPOs are seen when the spectrum is soft and L_X is high. The observations contaminated by a nearby HMXB are not included in the CD (see Section 2.3).

indicates whether the source is in the soft or hard state (as noted by Linares et al. 2009). This is probably due to hysteresis effects, which are typical for this type of systems (Maccarone & Coppi 2003; Meyer-Hofmeister, Liu & Meyer 2005).

3.2 Aperiodic variability

We examined all the power spectra in the energy band 3–30 keV individually for variability. We detect significant ($>3\sigma$ single-trial) QPOs in three different observations, the times of which are marked with arrows in the upper panel of Fig. 2. In Fig. 3, we indicate only the two uncontaminated observations of 2008. It should be noted that all these three QPOs were detected during the high-intensity state. The source is in the soft state during observations 93444-01-02-00 and 93444-01-04-00 (Fig. 3); the spectral state during the observation 95328-01-06-00 is difficult to constrain as the spectra are contaminated by an HMXB in the FoV (OAO 1657–415; see Section 2.3).

In the observation 93444-01-02-00 (MJD 546 33.2), we detect two QPOs at characteristic frequencies 30 ± 0.3 and 1152 ± 5 Hz. In Fig. 4, we show them separately for clarity. The 30 ± 0.3 Hz QPO is accompanied by a broad noise component fitted with a Lorentzian centred at 17.2 ± 5.9 Hz. In observations 93444-01-04-00 (MJD 546 65.1) and 95328-01-06-00 (MJD 554 25.08), we detect twin kHz QPOs at characteristic frequencies $\nu_\ell = 740 \pm 2$ and 738 ± 9 Hz and $\nu_u = 1112 \pm 17$ and 1098 ± 5 Hz, respectively (see Fig. 5). In the latter case (95328-01-06-00), we also detect a broad bump at 26.3 ± 5.6 Hz and a fractional rms amplitude of ~ 11 per cent. In the observation 93444-01-04-00, this broad bump is not detected significantly, with a 3σ upper limit of 19 per cent fractional rms amplitude. The difference in the centroid frequencies of the twin kHz QPOs is $\Delta\nu = 385 \pm 13$ and 360 ± 10 Hz for the two observations, respectively. In Table 2, we report on the best-fitting parameters for the detected features with single-trial significance $>3\sigma$.

To calculate the total number of trials, we use the fact that we looked for QPOs in the 0.1–2000 Hz range in 58 observations,

and that we found QPOs with FWHM as reported in Table 2. This leads to total numbers of trials 3170, 1574 and 2187 for observations 93444-01-02-00, 93444-01-04-00 and 95328-01-06-00, respectively. Under these conservative assumptions, the upper kHz QPOs in 93444-01-02-00 and 95328-01-06-00 are at 4.8 and 6.6σ , respectively, while the significance of all other QPOs including lower kHz QPOs is below 3σ . However, in atoll sources, the upper kHz QPOs are mostly detected in the high-luminosity soft state and in a narrower frequency range (800–1200 Hz); when we consider only the 12 soft-state observations (see Table 1 and Fig. 3), our numbers of trials are 131, 65 and 91, respectively, for the upper kHz QPOs detected in 93444-01-02-00, 93444-01-04-00 and 95328-01-06-00. With these considerations, the upper kHz QPOs in 93444-01-02-00 and 95328-01-06-00 have significances of 5.4σ and 3.8σ , respectively; the significance of the upper kHz QPO in 93444-01-04-00 falls to 1.6σ and that of the two detections of the lower kHz QPOs to $\sim 1\sigma$. However, since all kHz QPOs are detected in the soft state and in the expected frequency range for NSs (Wijnands & van der Klis 1997; Tomsick et al. 1999; Boirin et al. 2000; van Straaten et al. 2000, 2003; Jonker et al. 2001; Kaaret et al. 2002; Belloni et al. 2005; van der Klis 2006a; Altamirano et al. 2008b), we conclude that our kHz QPO detections in XTE J1701–407 are most probably real.

Apart from the QPO detections and the broad features mentioned above, we did not detect any of the other broad-band noise components expected in the banana state (e.g. van Straaten et al. 2003, 2005; Altamirano et al. 2008b). This is probably due to the low statistics in our data. To further investigate this, we averaged all the power spectra in two groups using only data when the source was either in the hard or in the soft state. In Fig. 6, we show the averaged power spectrum of all hard-state observations; the power spectrum has a 0.1–100 Hz integrated fractional rms amplitude of 23.07 ± 1.17 per cent and it is well described with two broad noise components with characteristic frequencies ~ 0.52 and ~ 20.6 Hz (see Table 3 for the best-fitting parameters). The quality factor Q is needed to be fixed to zero in our fits (as the best fit gave negative

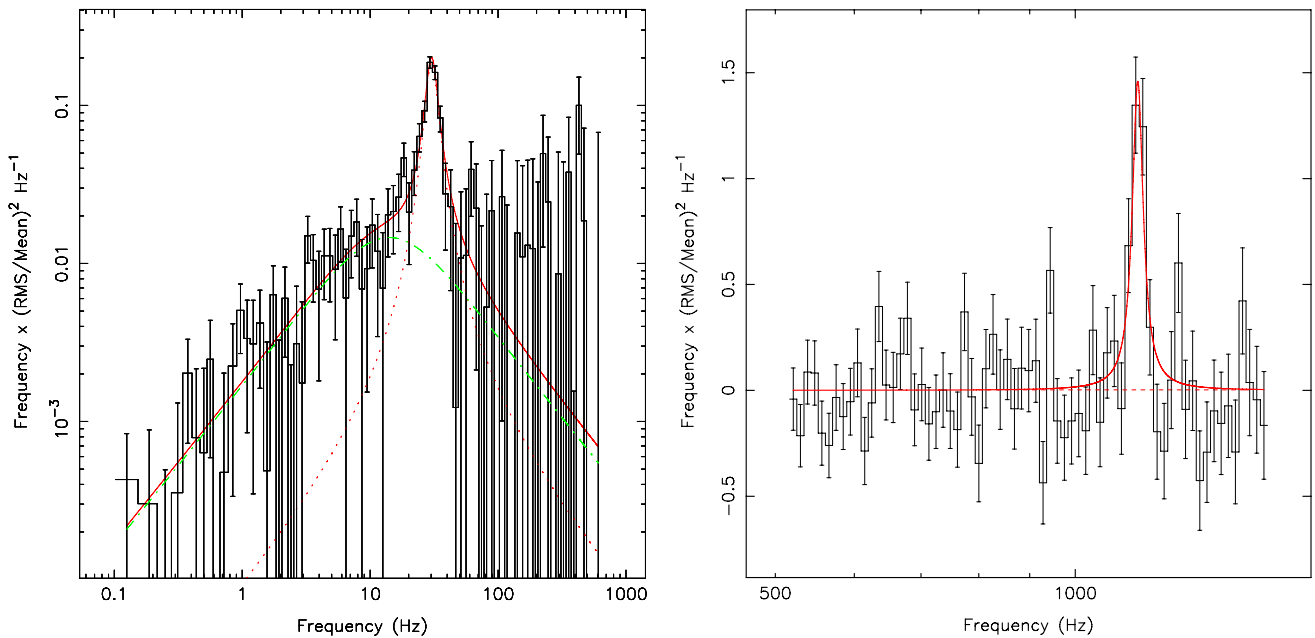


Figure 4. QPOs detected simultaneously in the observation 93444-01-02-00. For clarity, in the left-hand panel we show the low-frequency part of the power spectra (QPO is at 30.4 ± 0.3 Hz) and in the right-hand panel we show the kHz QPO ($\nu = 1152.7 \pm 5.2$ Hz). The average count rate in this observation is 39.6 cts/s/PCU after correcting for the background; two detectors were on during this observation.

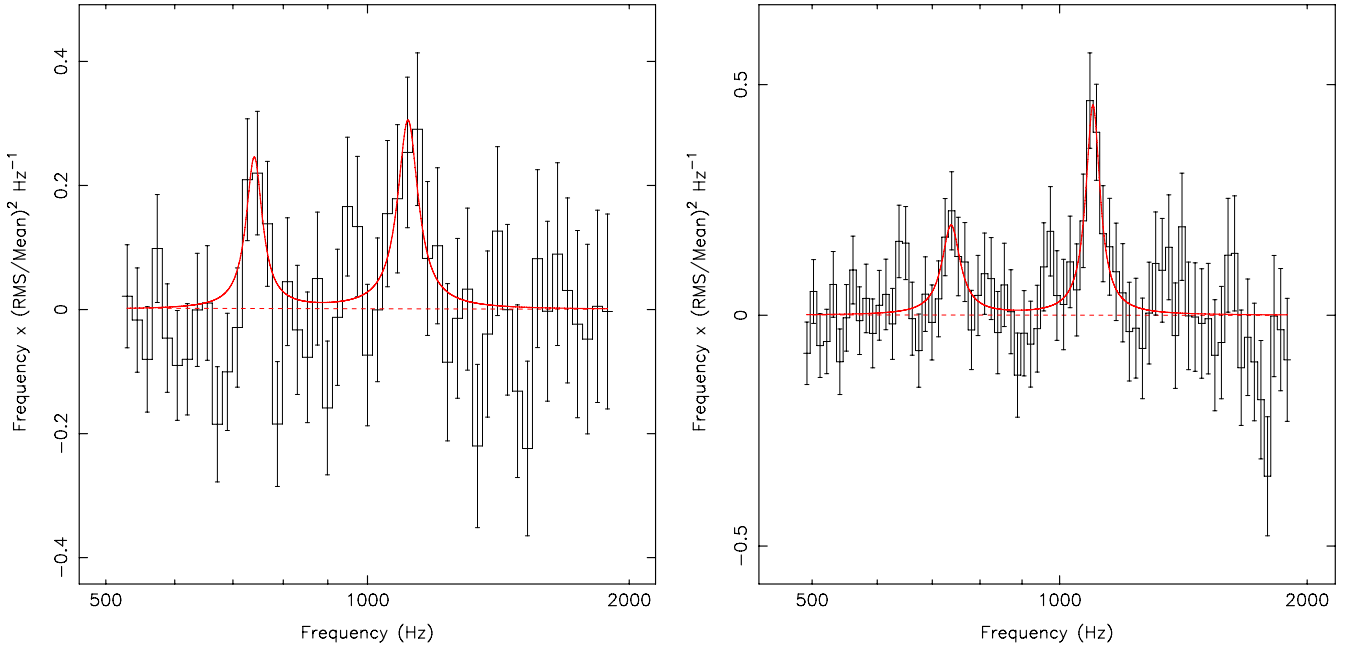


Figure 5. Left-hand panel: twin kHz QPOs observed simultaneously in the observation 93444-01-04-00 (at 740.8 ± 2.6 and 1112.6 ± 17.0 Hz). The average count rate per detector in this observation is 41.7 cts/s/PCU after correcting for the background. Two detectors were on during this observation. Right-hand panel: twin kHz QPOs observed simultaneously in the observation 95328-01-06-00 (at 740.5 ± 11.7 and 1097.8 ± 5.8 Hz). The average count rate per detector in this observation is 54.5 cts/s/PCU after correcting for the background and two detectors were on during this observation.

Table 2. QPO parameters in the energy range 3–30 keV.

Observation	ν_{\max} (Hz)	rms (per cent)	Q
93444-01-02-00	17.2 ± 5.9	20.9 ± 3.3	0.09 ± 0.25
	30.3 ± 0.3	25.8 ± 1.7	4.3 ± 0.7
	1152.7 ± 5.2	26.8 ± 2.2	31.5 ± 10.6
93444-01-04-00	740.8 ± 2.6	11.2 ± 1.6	15.1 ± 9.2
	1112.6 ± 17.0	17.7 ± 3.2	15.1 ± 9.4
95328-01-06-00	26.3 ± 5.6	11.5 ± 1.7	0.7 ± 0.5
	740.5 ± 11.7	14.2 ± 2.3	13.1 ± 7.4
	1097.8 ± 5.8	18.5 ± 1.9	20.7 ± 5.7

values; note that this is common practice when the component is too broad and is consistent with a Lorentzian of $\nu_0 = 0$ Hz; see, e.g., Belloni et al. 2002; van Straaten et al. 2005); we note that the frequency ν and fractional rms did not change significantly before and after the value of Q was fixed. The averaged power spectrum of the soft-state observations (excluding the contaminated observations and those in which we detect QPOs) has a 0.1–100 Hz integrated fractional rms amplitude of 7.16 ± 1.61 per cent and shows no significant features; we detected only an ~ 50 Hz signal with a significance of 2.6σ . For this power spectrum, we estimated 7.01, 13.4 and 12.6 per cent confidence upper limits for ~ 30 , ~ 740 and ~ 1110 Hz QPOs, respectively, with parameters similar to those in Table 2.

3.3 Correlation of ν_{ii} and the other characteristic frequencies

The characteristic frequencies of the various power spectral components (so-called L_b , L_{hHz} , L_{b2} , L_c) are correlated to the characteristic frequency ν_{ii} of the upper kHz QPO (see e.g. van Straaten et al. 2003, 2005; Altamirano et al. 2008b, and references within).

In Fig. 7, we plot the characteristic frequency of the various components versus ν_{ii} for XTE J1701–407, and for the atoll sources 4U

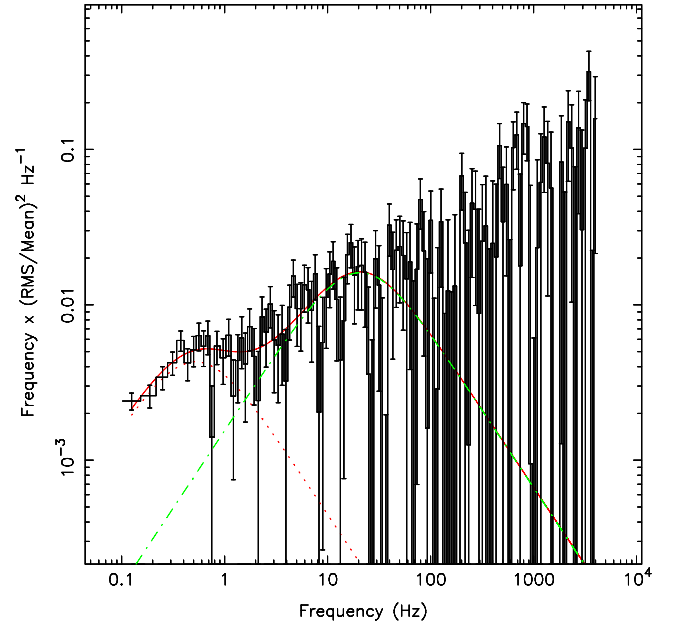


Figure 6. Broad-band noise detected in the power density spectrum calculated by adding all the hard-state observations. Fit parameters are given in Table 3. The average count rate in this observation is 31.7 cts/s/PCU after correcting for the background.

Table 3. Broad-band noise parameters measured in the averaged power spectrum of the hard-state observations (circles in the CD, Fig. 3); energy range 3–30 keV.

ν_{\max} (Hz)	rms (per cent)	Q
0.52 ± 0.07	11.6 ± 0.56	0(fixed)
20.6 ± 5.16	22.47 ± 1.5	0(fixed)

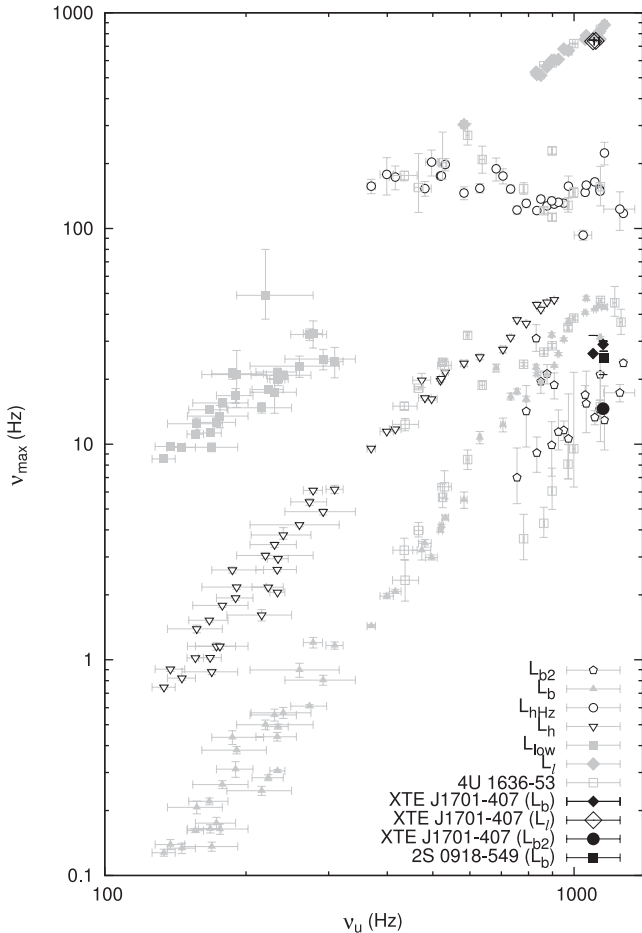


Figure 7. Characteristic frequency of the upper kHz QPO versus that of other QPO and noise components. The lower kHz QPO frequencies of XTE J1701–407 are represented with diamonds (they overlap) and the ~ 30 Hz QPOs are represented using filled black diamonds. The error bars are of the size of the symbols for the XTE J1701–407 points. We also include data for LMXB 2S 0918–549 from Jonker et al. (2001), where the 1156 ± 9 Hz QPO is accompanied by a peaked noise component of 25 ± 2 Hz. L_{b2} , L_b , L_{hHz} , L_h , L_{low} and L_l are the components of atoll sources 4U 0614+09, 4U 1608–52, 4U 1728–34 and Aql X–1 (van Straaten et al. 2003).

0614+09, 4U 1608–52 and 4U 1728–34 (van Straaten et al. 2003, 2005; Altamirano et al. 2005, 2008b). As can be seen, at high ν_u , different tracks blend together and sometimes it is difficult to differentiate between power spectral components. Our low-frequency features could be L_b or L_{b2} only based on the frequency correlations. The high coherence of the feature at ~ 30 Hz suggests that it might be L_b (see, e.g., Altamirano et al. 2008b).

3.4 Fractional rms amplitude versus luminosity

In Fig. 8, we show the fractional rms amplitude of the kHz QPOs versus the luminosity L_X/L_{Edd} for XTE J1701–407 and other sources. The fractional rms amplitude is calculated for the upper kHz QPO if it is significantly detected in the 5–60 keV range, and it is plotted for the maximum and minimum frequency of the upper kHz QPOs detected in each source (see Jonker et al. 2001). Besides the high dispersion of the data, it is clear that there is an anticorrelation between the fractional rms amplitude of the kHz QPOs and the source flux. The data of XTE J1701–407 are consistent with the anticorrelation [we estimated the rms amplitudes in the 5–60 keV range

to match the energy range used by Jonker et al. (2001)]. The flux upper limit used for XTE J1701–407 in Fig. 8 was obtained from Linares et al. (2009) and data for the other sources from Ford et al. (2000) and Jonker et al. (2001).

3.5 Correlation of rms and energy

The fractional rms amplitude of QPOs is a measure of the fraction of observed photons which are modulated at the QPO frequency, and so can give additional information useful to understand the physical process that sets the amplitude and/or the frequency of the oscillation (see Cabanac et al. 2010; Gierliński & Zdziarski 2005; Zdziarski 2005; Zdziarski et al. 2005, and references within for extensive discussion). The fractional rms amplitude of QPOs increases with energy (the only clear exceptions are the mHz QPOs in three atoll sources thought to be due to marginally stable burning of hydrogen or helium on the NS surface; see, e.g., Altamirano et al. 2008a; Revnivtsev et al. 2001, and references therein). In Fig. 9, we show the fractional rms amplitude versus energy of the kHz QPO at ~ 1112 Hz in the observation 93444-01-04-00. We plot two points (energy bands 2.06–5.71 and 6.12–31.7 keV; more points lead to larger errors). Points from the observation 93444-01-02-00 are not included because of very low statistics and points from 95328-01-06-00 are not included as it is one of the contaminated observations. For comparison we also include the data for the atoll source 4U 1608–52 (Berger et al. 1996; Méndez et al. 1998). We see that the rms depends weakly on energy for XTE J1701–407, significantly different from the relatively luminous source 4U 1608–52, where it increases monotonically with energy.

4 DISCUSSION

In this paper, we report the discovery of kHz QPOs in the LMXB XTE J1701–407. XTE J1701–407 is one of the least luminous LMXBs that show kHz QPOs at an average flux of $\approx 3 \times 10^{-10}$ erg cm $^{-2}$ s $^{-1}$ in the 2–20 keV band (Falanga et al. 2009); from time to time it shows a sudden excursion to the soft state as the source intensity increases. The increased emission is most probably because of an increase in the mass accretion rate (\dot{M}). When \dot{M} increases, it leads to high L_X and the spectrum softens. This is a well-known behaviour in compact accreting objects, (see, e.g., Done & Gierliński 2003; Done, Gierliński & Kubota 2007, and references within). Based on the transition tracks between hard and soft states in the CD, Gladstone, Done & Gierliński (2007) have classified atoll sources as diagonals and verticals. Comparison of the first and last panels of Fig. 3 with the second row of fig. 2 in Gladstone et al. (2007) implies that XTE J1701–407 behaves as a vertical. According to Gladstone et al. (2007), this means \dot{M} is low enough to allow the magnetic field to emerge from the surface of the NS and affect the accretion flow. Given that the CD of XTE J1701–407 resembles that seen in other low-luminosity sources, it shows thermonuclear X-ray bursts (Markwardt et al. 2008; Falanga et al. 2009; Linares et al. 2009; Chenevez et al. 2010), strong broadband noise in the hard state and kHz QPOs when the source flux is highest and spectra softest, we conclude that XTE J1701–407 can be classified as an atoll source (see also Linares et al. 2009).

4.1 Quasi-periodic oscillations

Twin kHz QPOs were detected on two occasions with centroid frequency differences of $\Delta\nu = 385 \pm 13$ and 360 ± 10 Hz, i.e. $\Delta\nu$ is the same within errors in both cases. This $\Delta\nu$ is among

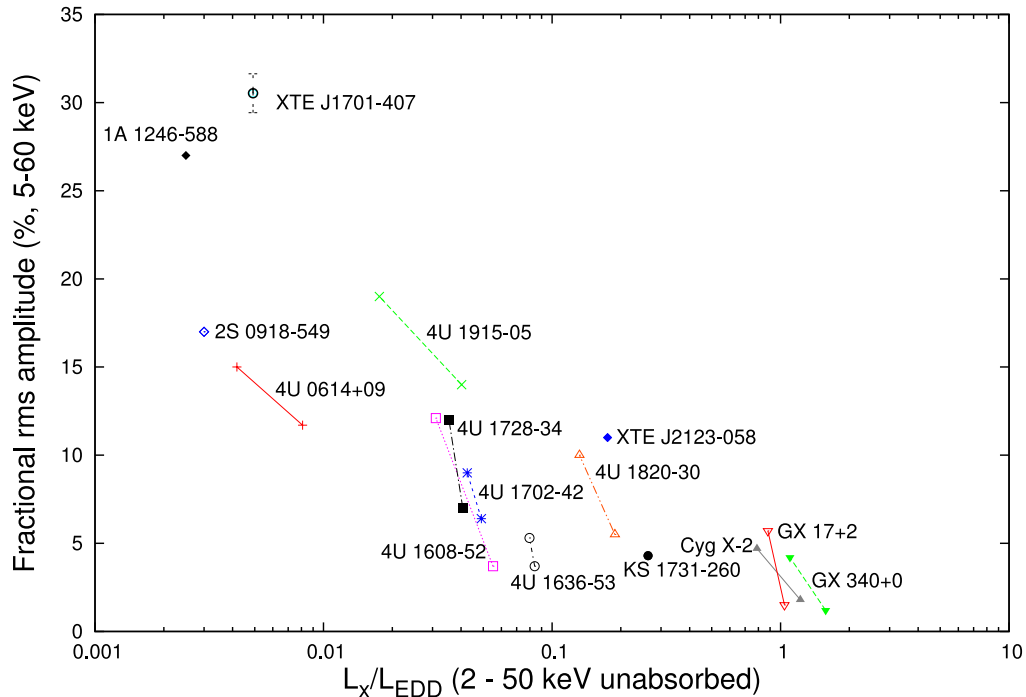


Figure 8. Luminosity versus fractional rms amplitude (5–60 keV) of the upper kHz QPO in various LMXBs from Jonker et al. (2001). We also include the data for 1A 1246–588 from Jonker et al. (2007) and for XTE J1701–407 from our analysis. The L_X/L_{Edd} for XTE J1701–407 is calculated using a distance of 5.0 ± 0.4 kpc from Chenevez et al. (2010); the error bars for L_X/L_{Edd} are much smaller than the size of the symbols.

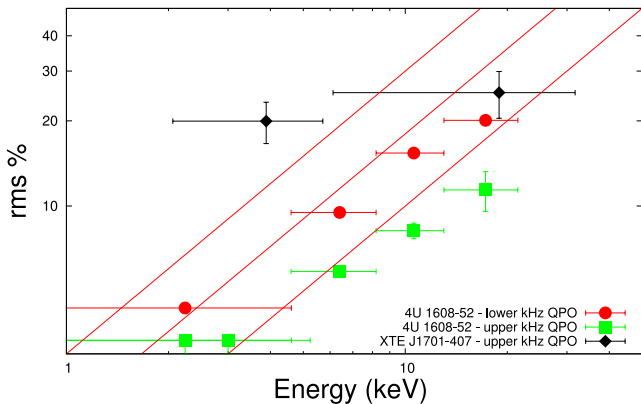


Figure 9. Energy dependence of the fractional rms amplitude of the upper kHz QPO in XTE J1701–407 (filled black diamonds) compared with 4U 1608–52, L_ℓ (filled circles) and L_u (filled squares) (Berger et al. 1996; Méndez et al. 1998). The error bars on rms for the filled circles are smaller than the size of the symbols. We overplot reference lines given by $f(x) = ax$, where $a = 1, 1.8, 3$.

the highest detected in an NS LMXB so far (van der Klis et al. 1997; van der Klis 2000; Méndez & Belloni 2007); the other higher values are $\Delta\nu = 413 \pm 20$ Hz in GX 340+0 (Jonker, Méndez & van der Klis 2000) and $\Delta\nu = 378 \pm 25$ Hz in 4U 0614+09 (van Straaten et al. 2000). Occurrences of high $\Delta\nu$ highlight the fact that models for kHz QPOs should be able to accommodate $\Delta\nu$ values from ~ 190 Hz (Linares et al. 2005) up to ~ 400 Hz.

Although it is still not confirmed nor refuted (see, e.g., Méndez & Belloni 2007; van der Klis 2008), it has been proposed that $\Delta\nu$ is related to the spin frequency ν_s of the NS (Strohmayer et al. 1996; Miller et al. 1998). Muno et al. (2001), based on observational results, proposed that $\Delta\nu \simeq \nu_s$ (for $\nu_s \lesssim 400$) and $\Delta\nu \simeq \nu_s/2$ (for

$\nu_s \gtrsim 400$). The spin frequency of the NS in XTE J1701–407 is not known; however, assuming that the proposal of Muno et al. (2001) is correct, the spin frequency of XTE J1701–407 should be around 185 Hz or around 370 Hz.

4.2 kHz QPO fractional rms amplitude versus luminosity

Jonker et al. (2001) showed that there was an anticorrelation between the kHz QPO fractional rms amplitude and the X-ray luminosity L_X of the source when the QPOs were detected. This was further supported by the results of Jonker et al. (2007), who found 27 ± 3 per cent fractional rms amplitude kHz QPOs in the low-luminosity NS 1A 1246–588. As shown in Fig. 8, our discovery of kHz QPOs on XTE J1701–407 further supports the anticorrelation. As can be seen, the anticorrelation has some dispersion, and although kHz QPOs have been detected in sources at lower L_X than XTE J1701–407 (e.g. 4U 0614+109 and 2S 0918–549), the kHz QPO fractional rms amplitude in XTE J1701–407 is the highest rms reported as yet for an upper kHz QPO. To date there is no clear picture that explains this anticorrelation (e.g. Jonker et al. 2001, 2007) and, as suggested by Jonker et al. (2001), it should be considered when modelling the mechanisms producing the kHz QPOs.

Méndez (2006) studied the relation between the maximum fractional rms amplitude of the kHz QPOs observed in a source and the source luminosity, and found that for the upper kHz QPO, the fractional rms amplitude was approximately constant (~ 20 per cent) at $<0.1L_{\text{Edd}}$ (2–60 keV), and decreased at $>0.1L_{\text{Edd}}$ (see fig. 3 of Méndez 2006). The results on the kHz QPO in 1A 1246–588 by Jonker et al. (2007) cast doubt on this trend, and led those authors to the conclusion that either the relation between kHz QPO frequency and fractional rms is significantly different in 1A 1246–588 from that which is seen in other NS LMXBs or the increase in amplitude and source luminosity does not level off at ~ 20 per cent (Méndez

2006) but keeps increasing. Our results on the kHz QPOs in XTE J1701–407 have a fractional rms amplitude of 30.5 ± 1.1 per cent (5–60 keV) when at ~ 1100 – 1150 Hz, showing that 1A 1246–588 is not unique, and strongly supporting the conjecture of Jonker et al. (2007) that the fractional rms amplitude keeps increasing at low luminosity.

ACKNOWLEDGEMENTS

DP and KS thank IUCAA, Pune, India, and University of Amsterdam, Netherlands, for their support and thank Ranjeev Misra and Gulab Dewangan for discussions during their visits to IUCAA. This research has made use of NASA's Astrophysics Data System. This research has made use of data obtained through the High Energy Astrophysics Science Archive Research Center Online Service, provided by the NASA/Goddard Space Flight Center.

REFERENCES

- Altamirano D., van der Klis M., Méndez M., Migliari S., Jonker P. G., Tiengo A., Zhang W., 2005, *ApJ*, 633, 358
- Altamirano D., van der Klis M., Wijnands R., Cumming A., 2008a, *ApJ*, 673, L35
- Altamirano D., van der Klis M., Méndez M., Jonker P. G., Klein-Wolt M., Lewin W. H. G., 2008b, *ApJ*, 685, 436
- Altamirano D. et al., 2010, *MNRAS*, 401, 223
- Barnstedt J. et al., 2008, *A&A*, 486, 293
- Belloni T., Psaltis D., van der Klis M., 2002, 572, 392
- Belloni T., Homan J., Casella P., van der Klis M., Nespoli E., Lewin W. H. G., Miller J. M., Méndez M., 2005, *A&A*, 440, 207
- Berger M. et al., 1996, *ApJ*, 469, L13
- Boirin L., Barret D., Olive J. F., Bloser P. F., Grindlay J. E., 2000, *A&A*, 361, 121
- Cabanac C., Henri G., Petrucci P. O., Malzac J., Ferreira J., Belloni T. M., 2010, *MNRAS*, 404, 738
- Chenevez J. et al., 2010, *Astron. Telegram*, 2814, 1
- Degenaar N., Wijnands R., Altamirano D., Cackett E., Linares M., Homan J., Fridriksson J., 2011a, *Astron. Telegram*, 3604, 1
- Degenaar N., Wijnands R., Altamirano D., Cackett E., Linares M., Homan J., Fridriksson J., 2011b, *Astron. Telegram*, 3654, 1
- Denis M., Bulik T., Marcinkowski R., 2010, *Acta Astron.*, 60, 75
- Di Salvo T., Méndez M., van der Klis M., 2003, *A&A*, 406, 177
- Done C., Gierliński M., 2003, *MNRAS*, 342, 1041
- Done C., Gierliński M., Kubota A., 2007, *A&AR*, 15, 1
- Falanga M., Cumming A., Bozzo E., Chenevez J., 2009, *A&A*, 496, 333
- Ford E. C., van der Klis M., Méndez M., Wijnands R., Homan J., Jonker P. G., van Paradijs J., 2000, *ApJ*, 537, 368
- Gierliński M., Zdziarski A. A., 2005, *MNRAS*, 363, 1349
- Gladstone J., Done C., Gierliński M., 2007, *MNRAS*, 378, 13
- Hasinger G., van der Klis M., 1989, *A&A*, 225, 79
- Homan J. et al., 2010, *ApJ*, 719, 201
- Jahoda K., Markwardt C. B., Radeva Y., Rots A. H., Stark M. J., Swank J. H., Strohmayer T. E., Zhang W., 2006, *ApJS*, 163, 401
- Jonker P. G., Méndez M., van der Klis M., 2000, *ApJ*, 540, L29
- Jonker P. G. et al., 2001, *ApJ*, 553, 335
- Jonker P. G., Méndez M., van der Klis M., 2002, *MNRAS*, 336, L1
- Jonker P. G., in't Zand J. J. M., Méndez M., van der Klis M., 2007, *MNRAS*, 378, 1187
- Kaaret P., in't Zand J. J. M., Heise J., Tomsick J. A., 2002, *ApJ*, 575, 1018
- Kaur R., Paul B., Raichur H., Sagar R., 2007, *ApJ*, 660, 1409
- Kuulkers E., van der Klis M., Oosterbroek T., Asai K., Dotani T., van Paradijs J., Lewin W. H. G., 1994, *A&A*, 289, 795
- Lamb F. K., Miller M. C., 2003, preprint (arXiv:astro-ph/0308179)
- Lee W. H., Abramowicz M. A., Kluźniak W., 2004, *ApJ*, 603, L93
- Linares M., van der Klis M., Altamirano D., Markwardt C. B., 2005, *ApJ*, 634, 1250
- Linares M., Watts A. L., Wijnands R., Soleri P., Degenaar N., Curran P. A., Starling R. L. C., van der Klis M., 2009, *MNRAS*, 392, L11
- Maccarone T. J., Coppi P. S., 2003, *MNRAS*, 338, 189
- Markwardt C. B., Swank J. H., 2003, *IAU Circ.*, 8144, 1
- Markwardt C. B., Pereira D., Swank J. H., 2008, *Astron. Telegram*, 1569, 1
- Méndez M., 2006, *MNRAS*, 371, 1925
- Méndez M., Belloni T., 2007, *MNRAS*, 381, 790
- Méndez M. et al., 1998, *ApJ*, 494, L65
- Meyer-Hofmeister E., Liu B. F., Meyer F., 2005, *A&A*, 432, 181
- Miller M. C., Lamb F. K., Psaltis D., 1998, *ApJ*, 508, 791
- Muno M. P., Chakrabarty D., Galloway D. K., Savov P., 2001, *ApJ*, 553, L157
- Psaltis D., Belloni T., van der Klis M., 1999, *ApJ*, 520, 262
- Revnivtsev M., Churazov E., Gilfanov M., Sunyaev R., 2001, *A&A*, 372, 138
- Schnerr R. S., Reerink T., van der Klis M., Homan J., Méndez M., Fender R. P., Kuulkers E., 2003, *A&A*, 406, 221
- Strohmayer T. E., Zhang W., Swank J. H., Smale A., Titarchuk L., Day C., Lee U., 1996, *ApJ*, 469, L9
- Strohmayer T. E., Markwardt C. B., Swank J. H., 2008, *Astron. Telegram*, 1635, 1
- Swank J., Markwardt K., 2001, in Inoue H., Kunieda H., eds, *ASP Conf. Ser. Vol. 251, New Century of X-ray Astronomy*. Astron. Soc. Pac., San Francisco, p. 94
- Tomsick J. A., Halpern J. P., Kemp J., Kaaret P., 1999, *ApJ*, 521, 341
- van der Klis M., 1995a, in Giovannelli F., Mannocchi G., eds, *Vulcano Workshop 2008: Frontier Objects in Astrophysics and Particle Physics*. Kluwer, Dordrecht, p. 213
- van der Klis M., 1995b, in Alpar M. A., Kiziloglu U., van Paradijs J., eds, *Proc. NATO Advanced Study Institute on the Lives of the Neutron Stars, The Lives of the Neutron Stars*. Kluwer Academic, Dordrecht, p. 301
- van der Klis M., 2000, *ARA&A*, 38, 717
- van der Klis M., 2006a, *Rapid X-ray Variability*. Cambridge Univ. Press, Cambridge, p. 39
- van der Klis M., 2006b, in Lewin W. H. G., van der Klis M., eds, *Compact Stellar X-Ray Sources*. Cambridge Univ. Press, Cambridge, p. 39
- van der Klis M., 2008, in Wijnands R., Altamirano D., Soleri P., Degenaar N., Rea N., Casella P., Patruno A., Linares M., eds, *AIP Conf. Ser. Vol. 1068, A Decade of Accreting Millisecond X-Ray Pulsars*. Am. Inst. Phys., New York, p. 163
- van der Klis M., Wijnands R. A. D., Horne K., Chen W., 1997, *ApJ*, L97
- van Straaten S., Ford E. C., van der Klis M., Méndez M., Kaaret P., 2000, *ApJ*, 540, 1049
- van Straaten S., van der Klis M., Méndez M., 2003, *ApJ*, 596, 1155
- van Straaten S., van der Klis M., Wijnands R., 2004, *Nucl. Phys. B*, 132, 664
- van Straaten S., van der Klis M., Wijnands R., 2005, *ApJ*, 619, 455
- Wijnands R., Miller J. M., 2002, *ApJ*, 564, 974
- Wijnands R. A. D., van der Klis M., 1997, *ApJ*, 482, L65
- Wijnands R., van der Klis M., Homan J., Chakrabarty D., Markwardt C. B., Morgan E. H., 2003, *Nat*, 424, 44
- Yin H. X., Zhang C. M., Zhao Y. H., Lei Y. J., Qu J. L., Song L. M., Zhang F., 2007, *A&A*, 471, 381
- Zdziarski A. A., 2005, *MNRAS*, 360, 816
- Zdziarski A. A., Gierliński M., Rao A. R., Vadawale S. V., Mikołajewska J., 2005, *MNRAS*, 360, 825
- Zhang W., Giles A. B., Jahoda K., Soong Y., Swank J. H., Morgan E. H., 1993, in Siegmund O. H., ed., *Proc. SPIE, Vol. 2006, EUV, X-Ray, and Gamma-Ray Instrumentation for Astronomy IV*. SPIE, Bellingham, p. 324
- Zhang W., Jahoda K., Swank J. H., Morgan E. H., Giles A. B., 1995, *ApJ*, 449, 930